J Oceanogr (2017) 73:169–180
DOI 10.1007/s10872-016-0394-9

ORIGINAL ARTICLE

A note on a critical wind speed for air–sea boundary processes

Hisashi Mitsuyasu[1]

Received: 9 February 2016 / Revised: 22 September 2016 / Accepted: 5 October 2016 / Published online: 17 October 2016

Abstract Wind and wind-generated waves were measured in a wind-wave tank. A clear transition was found in the relation between the wind speed U_{10} and the wind friction velocity u_* near $u_* = 0.2$ m/s, where U_{10} is the wind speed at 10 m height extrapolated from the measured wind profile in a logarithmic layer, and $u_* = 0.2$ m/s corresponds roughly to $U_{10} = 8$ m/s in the present measurement. Quite a similar transition was found in the relation between the spectral density of high frequency wind waves and u_*. These results suggest the existence of the critical wind speed for air–sea boundary processes, which was proposed by Munk (J Marine Res 6:203–218, 1947) more than half a century ago. His original idea of the critical wind speed was based on the discontinuities in such phenomena as white caps, wind stress, and evaporation, which commonly appear at a wind speed near 7 m/s. On the basis of the results of our present study and those of earlier studies, we discuss the phenomena which are relevant to the critical wind speed for the air–sea boundary processes. The conclusion is that the critical wind speed exists and it is attributed to the start of wave breaking rather than the Kelvin–Helmholtz instability, but the air–sea boundary processes are not discontinuous at a particular wind speed; because of the stochastic nature of breaking waves, the changes occur over a range of wind speeds. Detailed discussions are presented on the dynamical processes associated with the critical wind speed such as wind-induced change of sea surface roughness and high frequency wave spectrum. Future studies are required, however, to clarify the dynamical processes quantitatively. In particular, there is a need to further examine the gradual change of breaking patterns of wind waves with the increase of wind speed, and the associated change of the structure of the wind over wind waves, such as separation of the airflow at the crest of wind waves, the turbulent stress, and wave-induced stress. Studies on the dynamical structure of the high frequency wave spectrum are also needed.

Keywords Air–sea boundary processes · Critical wind speed · Sea surface roughness · Breaking waves · High frequency wave spectrum

1 Introduction

More than half a century ago Munk (1947) proposed an attractive idea of the existence of the critical wind speed for air–sea boundary processes. His idea is based on discontinuities in the wind-speed dependence of such phenomena as white caps, soaring of birds, wind stress, and evaporation, all of which commonly appear at Beaufort 4 ($U_{10} = 5.5$–7.9 m/s). Furthermore he attributed the discontinuities to the change of sea surface roughness caused by unstable wavelets generated by the Kevin–Helmholtz (K–H) instability which occurs for wind speeds exceeding $U = 6.5$ m/s (Lamb 1932). Here U is a wind speed which has a vertically uniform distribution over the water surface. At that time, his idea was quite a new and consistent one that the unstable wavelet generated by the K–H instability changes sea surface roughness from smooth to rough, and the change appears abruptly at the critical wind speed for the generation of the K–H instability. However, data to support Munk's idea were few and not always accurate enough. Many later observations of the sea surface

✉ Hisashi Mitsuyasu
mi.tsu.ya.su-h@amber.plala.or.jp

[1] Kyushu University, Miwadai 4-16-12, Higashiku, Fukuoka 811-0212, Japan

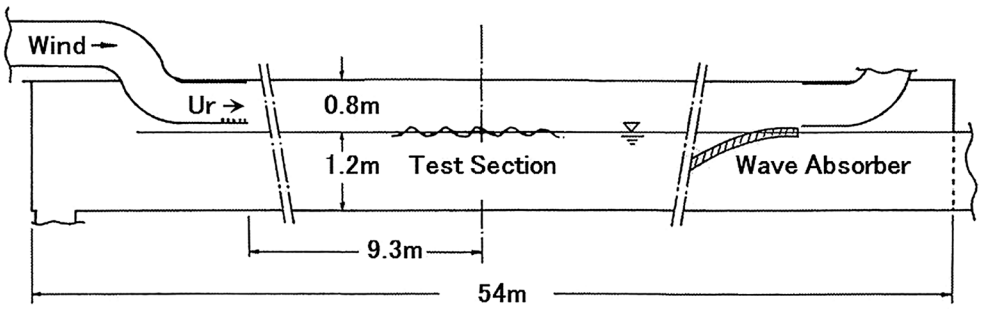

Fig. 1 Schematic figure of wind-wave tank. Wind and waves were measured at the fetch 9.3 m

roughness did not show a clear discontinuity. Furthermore, the idea for attributing the critical wind speed to the K–H instability has not been thoroughly investigated. More fundamentally Miles' (1959) study has shown that the K–H instability at the air–sea interface is unlikely at commonly observed wind speeds. Therefore, Munk's attractive idea has been gradually disregarded; no discussion is given in prominent texts such as Kinsman (1965), Phillips (1977), or Jones and Toba (2001), though quite recently Babanin (2009) referred in his review paper to Munk's study in the discussion of the wave-breaking probability.

In 1992, more than 20 years ago, we carried out an experimental study on air–sea boundary processes focused on microwave backscattering from the wind wave surface. The results of the study were published partly in two short papers: the proceedings of PORSEC '92 in Okinawa (Mitsuyasu et al. 1992) and that of PORSEC '98 in Qingdao (Mitsuyasu 1998). Recently, however, on looking closely at the data of our previous study we noticed the interesting fact that the wind speed U_{10} at 10 m height above the water surface, the spectral density $\mathbf{\Phi}(\mathbf{f})$ of high frequency wind waves ($f \geq 10$ Hz), and microwave backscattering cross section H_{HH}[1] show commonly quite similar changes against the wind friction velocity u_*, and their wind-speed dependence changes near the wind friction velocity $u_* = 0.2$ m/s. The friction velocity $u_* = 0.2$ m/s corresponds roughly to the wind speed U_{10} at 10 m height, of 8 m/s in our present study, and we naturally recall the existence of the critical wind speed for air–sea boundary processes which was proposed by Munk (1947) but later gradually disregarded as mentioned above.

Triggered by the new findings we performed a detailed analysis of the data of the wind and wind waves to clarify the properties of the critical wind speed in a modern context, and to find the dynamical processes behind it. In the analysis of the data we fully used the results of our earlier studies (Mitsuyasu and Honda 1975; Mitsuyasu and Kusaba 1984) which are closely related to the present study. The former contains photographic data showing fine structure of wind waves, in addition to the spectral data, and the latter shows fundamental properties of sea surface roughness including the effect of soluble surfactant on the air–sea boundary process.

In Sect. 2 we briefly describe the wind-wave tank and measurements of wind and waves in the tank. In Sect. 3 we present measured results of the wind and waves. In Sect. 4 we summarize important results of the experimental study. In Sect. 5 we discuss the present results in the context of the critical wind speed. In the discussion, to clarify the complicated phenomena relevant to the critical wind speed, in addition to the present results, we use the results of our earlier studies which contain additional and important information.

2 Experiment

2.1 Wind-wave tank

The experiment was carried out in a large wind-wave tank 54 m long, 1.5 m wide, and 2 m high, which is shown schematically in Fig. 1. More detailed figures are shown in Kusaba and Masuda (1988). The water depth was kept at 1.2 m in the present experiment. All measurements were performed at the fetch $X = 9.3$ m.

2.2 Measurements

Wind waves were measured by using a capacitance-type wave gauge. The capacitance wire is 0.2 mm in diameter. The gauge can measure high frequency wind waves up to approximately 60 Hz (Mitsuyasu and Honda 1974, 1975).

The vertical wind profile over the water surface at the center of the test section was measured by using a Pitot static tube which is fixed to a vertical traverse mechanism controlled with a personal computer. In order to avoid disturbance in the wind field by the wave measuring system, the measurements of the wind profiles were made independently of the measurements of wind waves under the same experimental conditions. The mean wind speed at each

[1] Results of the microwave backscattering are not included in the present paper to focus on the fluid dynamical problem.

Table 1 Wind data

U_r (m/s)	u_* (m/s)	$z_0 \times 10^5$ (m)	U_{10} (m/s)	$C_D \times 10^3$
2	0.130	9.87	3.74	1.20
3	0.179	12.2	5.01	1.25
4	0.194	4.20	6.00	1.05
6	0.210	0.44	7.68	0.75
8	0.331	2.61	10.6	0.98
10	0.548	23.7	14.6	1.40
12	0.763	68.2	18.3	1.74
14	1.020	164	22.2	2.11

U_r reference wind speed (wind speed at an inlet of the test area), u_* friction velocity of the wind, z_0 roughness length, U_{10} wind speed at 10 m height obtained by extrapolating the wind profile in a logarithmic layer, $C_D = (u_*/U_{10})^2$ drag coefficient over water surface

point (height) was determined as a time average of 5 min of fluctuating wind speed. The average time of 5 min was determined after several trials to obtain stable and reliable mean values (Kusaba and Masuda 1988).

The wind speeds tested in the study were $U_r = 2$, 3, 4, 6, 8, 10, 12, 14 (m/s). Here U_r is a reference wind speed which is measured at a center of the inlet of the test area of the wind-wave tank, and corresponds approximately to a cross-sectional mean wind speed at the test section, while the exact cross-sectional mean wind speed at the test section needs a small correction for the change of the cross-sectional areas. The relations of the reference wind speed U_r to the wind speed U_{10} at 10 m height above the water surface and the friction velocity of the wind u_* are shown in Table 1.

The measured signal of the wind waves was digitized at the frequency of 200 Hz and recorded on a tape recorder. Wind wave spectra were computed through an FFT method by using 2048 data of 60 samples for each wave data corresponding to each wind speed: the total length of the wave data for each wind speed is roughly 10 min. Sample mean of the spectra was taken for 60 wave spectra corresponding to a definite wind speed. Furthermore, a spectral filter was applied by taking a moving average of five successive line spectra in each case in order to increase the reliability. The degrees of freedom of the measured spectra are approximately 600.

3 Results

3.1 Wind profiles and water surface roughness

Vertical wind profiles measured over the water surface at the center of the test section are illustrated in Fig. 2. Each profile near the water surface shows the following logarithmic profile:

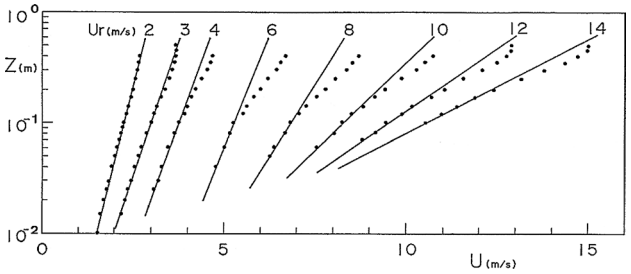

Fig. 2 Wind profiles over the wind wave surface. Reference wind speed U_r (m/s) is the wind speed at the inlet of the test area (see Fig. 1). *Dots* show measured wind speed and the *straight line* indicates the regression line for the logarithmic layer of the measured wind profile

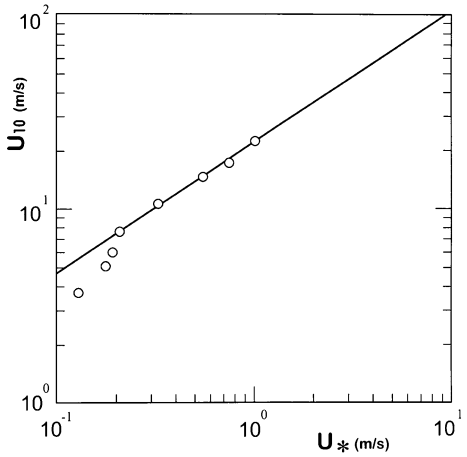

Fig. 3 Plot of the wind speed at 10 m height U_{10} versus the wind friction velocity u_*. The *straight line* indicates the regression line for the data in the region $u_* \geq 0.2$ m/s

$$U(z) = (u_*/\kappa) \ln (z/z_0), \tag{1}$$

where $U(z)$ is the mean wind speed at a height z, $u_* = (\tau/\rho)^{1/2}$ the wind friction velocity (τ is the wind shear stress, ρ is the density of air), κ the von Kármán constant, and z_0 the roughness length.

The wind friction velocity u_*, the roughness length z_0, and the wind speed U_{10} at 10 m height above the water surface were determined from the wind profiles in a logarithmic layer by the least square method by choosing $\kappa = 0.4$. The results are summarized in Table 1, where the drag coefficient C_D obtained as $(u_*/U_{10})^2$ is included. Note that U_{10} is the wind speed extrapolated from the wind profile in the logarithmic layer.

Figure 3 shows the relation between u_* and U_{10} in the present study. It is very interesting that the relation changes near the wind friction velocity $u_* = 0.2$ m/s ($U_{10} \fallingdotseq 8$ m/s). In a higher wind-speed region, $u_* \geq 0.2$ m/s, the relation can be approximated by the form

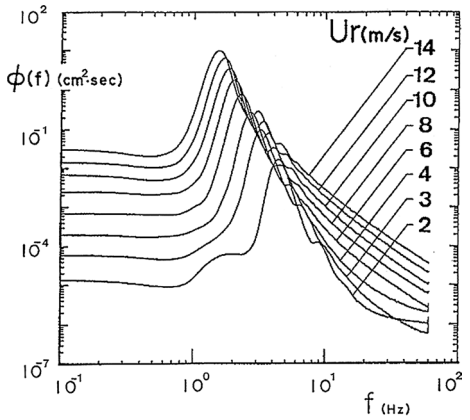

Fig. 4 Evolution of frequency spectrum of wind waves with wind speed at the fetch $X = 9.3$ m. Reference wind speed U_r (m/s): 2, 3, 4, 6, 8, 10, 12, 14

$$U_{10} = 21.9\, u_*^{0.668}, \tag{2}$$

in units of m/s.

Furthermore, from the definition of the drag coefficient $C_D = (u_*/U_{10})^2$ we can derive the following equation from Eq. (2) for the region $u_* \geq 0.2$ m/s:

$$C_D = 9.64 \times 10^{-5} U_{10}^{0.996}. \tag{3}$$

According to Eq. (3) the drag coefficient C_D over the water surface increases gradually with the increase of the wind speed U_{10} in the region $u_* \geq 0.2$ m/s ($U_{10} \geq 8$ m/s). However, in the region $u_* \leq 0.2$ m/s ($U_{10} \leq 8$ m/s), the drag coefficient over the water surface decreases with the increase of the wind speed U_{10}, as shown in Table 1. Dynamical processes relevant to these results will be discussed in Sect. 5.

3.2 Wind-induced growth of high frequency wave spectrum

Figure 4 shows the wind-induced growth of the frequency spectrum $\Phi(f)$ of wind waves measured at the center of the test section in the wind-wave tank. As previously found by Mitsuyasu and Honda (1974, 1975), wave spectral densities in a high frequency region, say 10 Hz $< f <$ 60 Hz, increase clearly with wind speed.

The wind-speed dependence of the present wave spectrum in a high frequency region has been studied in a way different from the previous one (Mitsuyasu and Honda 1974, 1975). We selected wave spectral densities $\Phi(10)$ and $\Phi(12)$, respectively, at $f = 10$ Hz and $f = 12$ Hz,[2] and correlated them with the wind friction velocity u_*. The results are shown in Fig. 5a, b.

It is very interesting that the dependence of the spectral densities of high frequency wave components on the wind friction velocity u_* is quite similar to the dependence of the wind speed U_{10} at 10 m height on the wind friction velocity u_*, which is shown in Fig. 3; the relations both change character near the wind friction velocity $u_* = 0.2$ m/s.

In the higher wind-speed region, $u_* \geq 0.2$ m/s, the following simple power law relation can be obtained from the results shown in Fig. 5a, b:

$$\Phi(\mathrm{f}) = \mathrm{A}\, \mathrm{u}_*^{\mathrm{B}}, \ (f : 10\,\mathrm{Hz},\ 12\ \mathrm{Hz}). \tag{4}$$

The values of the exponents B were 1.45 for $\Phi(10)$ and 1.55 for $\Phi(12)$: the exponent B seems to depend weakly on the frequency f.

Laboratory data of the wave number spectra obtained by Jähne and Riemer (1990) show quite similar changes to ours: their relation between spectral densities of high wave number spectra and the friction velocity u_* shows the transition near the friction velocity $u_* = 0.2$ m/s. In contrast, for ocean wave data obtained by Hara et al. (1994), the transition of spectral densities of high wave number spectra is seen near the friction velocity $u_* = 0.1$ m/s (cf. Fig. 4d in their paper), though their ocean data scatter considerably.

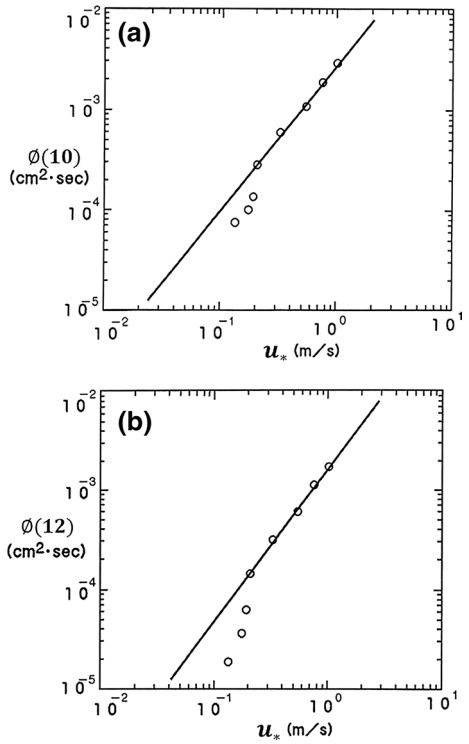

Fig. 5 Spectral density at 10 Hz, $\varphi_{(10)}$ (**a**), 12 Hz, $\varphi_{(12)}$ (**b**), versus the wind friction velocity u_*. The *straight line* indicates the regression line for the data in the region $u_* \geq 0.2$ m/s

[2] Selection of these spectral components of high frequency waves is due to the study on backscattering of microwaves of 9.6 GHz (wavelength $\lambda = 3.12$ cm) from wind wave surface.

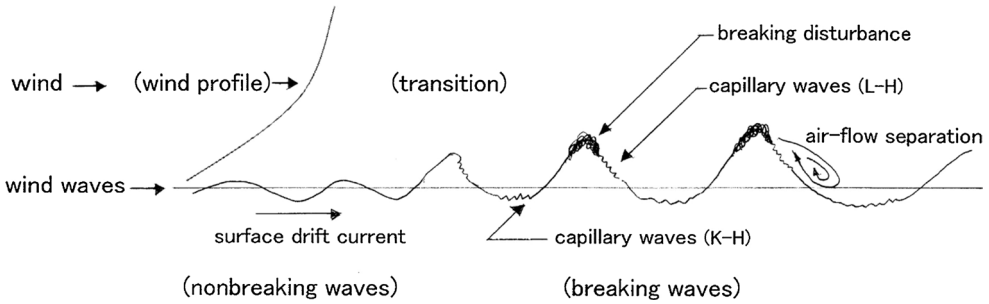

Fig. 6 Scheme explaining the phenomena in the air–sea boundary processes discussed in the present study. *K–H* the Kelvin–Helmholtz instability, *L–H* the Longuet–Higgins mechanism

Why the oceanic phenomena differ from those in the laboratory tanks is not clear.

4 Summary of results

Important results of the present experimental study are summarized as follows:

1. As shown in Fig. 3 the relation between the wind friction velocity u_* and the wind speed U_{10} at 10 m height above the water surface changes near the wind speed $u_* = 0.2$ m/s ($U_{10} \fallingdotseq 8$ m/s). In a higher wind-speed region, $u_* \geq 0.2$ m/s, the relation between u_* and U_{10} shows a simple power law. The result means that the air–sea boundary process changes near the wind speed $u_* = 0.2$ m/s ($U_{10} \fallingdotseq 8$ m/s). Furthermore, in the region $u_* \geq 0.2$ m/s, sea surface roughness increases with the increase of the wind speed (Eq. 3), while in the lower wind-speed region $u_* \leq 0.2$ m/s, sea surface roughness decreases with the increase of the wind speed (Table 1).
2. As shown in Fig. 5a, b quite a similar property is seen in the relation between the spectral density $\Phi(f)$ of high frequency wind wave component and the friction velocity of the wind u_*: the relation between $\Phi(f)$ and u_* changes near the wind speed $u_* = 0.2$ m/s ($U_{10} \fallingdotseq 8$ m/s), and in the higher wind-speed region $u_* \geq 0.2$ m/s, the relation shows a simple power law. Furthermore, in the region $u_* \geq 0.2$ m/s, the spectral density of high frequency wind wave component increases with the increase of the wind speed (Eq. 4).

That is, two different quantities, the wind speed U_{10} at 10 m height and the spectral density $\Phi(f)$ of high frequency wind wave component, commonly show quite similar changes against the wind friction velocity u_*: both relations change their trends near the wind speed $u_* = 0.2$ m/s ($U_{10} \fallingdotseq 8$ m/s) and show simple power laws in the wind-speed region $u_* \geq 0.2$ m/s.

The results suggest that a transition of the phenomena in air–sea boundary processes appears near the wind speed $u_* = 0.2$ m/s ($U_{10} \fallingdotseq 8$ m/s) and that sea surface roughness is intimately related to the high frequency components of wind waves.

5 Discussions

5.1 Overview of phenomena relevant to the present study

Before detailed discussions on the results of the present study we show in Fig. 6 the phenomena in the air–sea boundary processes which we are dealing with. Wind blowing over the water surface generates wind waves and surface drift current. The wind waves generated by low speed wind are small in size and nonbreaking, but they develop and their size increases with wind speed and fetch (distance from an upwind boundary). Furthermore, developed wind waves are generally breaking and covered with short ripples and turbulent disturbances generated mainly by wave breaking.

Corresponding to the growth of wind waves the wind blowing over the wind waves changes their properties: wind profile, wind shear stress, wave-induced stress, and turbulent structure change considerably. In such a way wind and wind waves are in an equilibrium state in the present experiment.

5.2 Relation between u_* and U_{10}

To clarify the dynamical processes for the change of the relation between u_* and U_{10} as shown in Fig. 3, the present data are compared with those of our earlier studies (Mitsuyasu and Kusaba 1984; Mitsuyasu and Honda 1986).

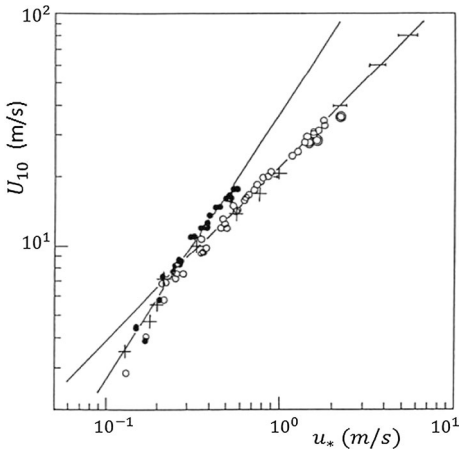

Fig. 7 Plot of the wind speed at 10 m height U_{10} versus the friction velocity u_*. Note that the vertical and horizontal axes are swapped in this figure from those in Fig. 3 of Mitsuyasu and Kusaba (1984). *Plus symbols* the present data; *unfilled circles* wind wave surface and *filled circles* data for the smooth and flat water surface from Mitsuyasu and Kusaba (1984); ⊙ data from Miller (1964); — data from Kunishi and Imasato (1966). The *straight lines* indicate regression lines for the data of wind wave surface and those for the smooth and flat water surface (steeper inclination)

In the earlier studies, wind profiles over the water surface were measured under two typical surface conditions: ordinary wind wave surface and smooth and flat water surface artificially generated by using soluble surfactant. Therefore, the earlier results are helpful in examining the dynamical processes for the sea surface roughness as reference data.

Figure 7 shows the relations between u_* and U_{10} both for the present study and for the earlier study (Mitsuyasu and Kusaba 1984). The present data shown in Table 1 and Fig. 3 were plotted in Fig. 7 with a symbol cross, superimposed on the earlier data. Note that the vertical and horizontal axes are swapped from those in the figure of the earlier study (Mitsuyasu and Kusaba 1984).

As shown in Fig. 7 the earlier data for the wind wave surface fit the present data well, though the earlier data were obtained in a different (smaller) wind-wave tank. The size of the wind-wave tank in the earlier study is 0.8 m high and 0.6 m wide with a test section length 15 m: the height and the width are less than half of the present ones.

In the following sections, we discuss the phenomena in the lower wind-speed region $u_* \leq 0.2$ m/s and those in the higher wind-speed region $u_* \geq 0.2$ m/s separately, because the dynamical process in each region is considered to be different.

5.2.1 Lower wind-speed region, $u_* \leq 0.2$ m/s

It is notable in Fig. 7 that in this region, $u_* \leq 0.2$ m/s, the relation between u_* and U_{10} is almost the same both for the wind wave surfaces (present and earlier) and for the smooth and flat water surface. The result means that the wind wave surface shows properties of an aerodynamically smooth surface in the lower wind-speed region, $u_* \leq 0.2$ m/s, even though small wind waves are generated. In other words, wind waves generated by relatively low wind-speed, $u_* \leq 0.2$ m/s ($U_{10} \leq 8$ m/s), do not contribute to water surface roughness.

It has long been said that water surface is aerodynamically smooth for low wind speed (e.g., Deacon and Webb 1962; Phillips 1977; Smith 1988), but becomes rough with the increase of wind speed. However, definitive data have not been shown as far as the author knows. The present result including the earlier one shown in Fig. 7 proves the idea for low wind speed clearly and quantitatively. Furthermore we can say from the present result that nonbreaking wind waves generated by relatively low wind speed are ineffective for the surface roughness.[3]

Regarding sea surface wind in the open ocean, Yelland and Taylor (1996) obtained data that are quite similar to ours: their result of sea surface roughness for low wind speed, $U_{10} \leq 6$ m/s, clearly shows the properties of a smooth surface: sea surface roughness decreases with the increase of wind speed. Their study also shows the existence of the critical wind speed of $U_{10} = 6$ m/s.

5.2.2 Higher wind-speed region, $u_* \geq 0.2$ m/s

As shown in Fig. 7, in the higher wind-speed region, $u_* \geq 0.2$ m/s, the relation between u_* and U_{10} for the wind wave surface (present and earlier) is very different from that for the smooth and flat water surface. The friction velocity u_* corresponding to the wind speed U_{10} is larger for the wind wave surface than that for the smooth and flat water surface. Since $u_* = (C_D)^{1/2}\ U_{10}$, the drag coefficient C_D of the wind wave surface is larger than that of the smooth and flat water surface.

Furthermore the drag coefficient of the wind wave surface in this region increases gradually with wind speed as shown in Eq. (3). Many similar results have been reported previously by many authors as shown in our earlier paper (Mitsuyasu and Kusaba 1984), but persuasive conclusions on the dynamical processes relevant to those results have not been presented yet. In the following discussion we

[3] The present author once measured the wind profile over the mechanically generated water waves with smooth surface, where the generation of wind waves was suppressed by using a soluble surfactant. It was found that the wind profiles were little affected by the water waves with smooth surface, and the drag coefficient over the water waves was almost the same as that over the smooth and flat water surface. The result is not published yet.

investigate the dynamical process for the gradual increase of sea surface roughness with the increase of wind speed.

Many years ago Banner and Melville (1976) and Banner (1990) performed ingenious laboratory experiments on wave breaking and showed that wave breaking triggers airflow separation at the crest of water waves. Furthermore Banner (1990) showed that breaking waves considerably increased the surface roughness. Therefore, it is certain that the increase of sea surface roughness in the higher wind-speed region shown in Fig. 7 is attributed to wave breaking.

On the other hand, there have been many studies showing that breaking probability and whitecap coverage increase with wind speed (e.g., Thorpe and Humphries 1980; Holthuijsen and Herbers 1986; Banner et al. 2000; Babanin et al. 2001; Zao and Toba 2001; Sugihara et al. 2007), where the breaking probability refers to the relative period of wave breaking at a special point, while the whitecap coverage refers to the relative spatial coverage at a particular moment. Since the phenomena are closely connected to our present study, we investigate briefly the mechanism generating them.

We consider the fetch-limited wind waves in a local equilibrium state, such as the present laboratory wind waves. From the fetch relations for wind wave energy E and spectral peak frequency ω_p, we can obtain the following form for the steepness of significant wind waves, H_S/L_S, as a function of the dimensionless fetch gX/U_{10}^2 (Mitsuyasu 1985):

$$H_S/L_S = 4E^{1/2}/L_S = 1.12 \times 10^{-1}\left(gX/U_{10}^2\right)^{-1/6}. \quad (5)$$

Here H_S ($=4E^{1/2}$) is the significant wave height (the mean of the highest one-third of the wave height in the wave record), Ls ($\simeq 2\pi g/\omega_p^2$) corresponds approximately to the significant wave length, g the gravitational acceleration, and X the fetch.

It can be seen from Eq. (5) that the steepness H_S/L_S of the dominant (significant) wind waves decreases with the increase of the dimensionless fetch gX/U_{10}^2. In another form, however, the significant wave steepness H_S/L_S is proportional to $(U_{10}^2/gX)^{1/6}$: the significant wave steepness increases with wind speed for a fixed fetch.

If the significant wave steepness continues to increase with the wind, the significant wave becomes unstable and starts to break. Furthermore, the breaking probability of wind waves increases with the increase of the significant wave steepness with the wind. Although the significant wave is a kind of averaged wave, the increase of the significant wave steepness is closely connected with the steepness of individual waves. The wind-speed dependence of wave breaking probability or whitecap coverage is caused by such a mechanism.

5.2.3 Wind-speed dependence of sea surface roughness

From the above discussions that wave breaking increases considerably sea surface roughness and breaking probability increases with the increase of wind speed, we can obtain the following simple dynamical model for the wind-speed dependence of the sea surface roughness:

(1) Increase of wind speed → (2) increase of wave steepness → (3) increase of wave breaking probability → (4) increase of sea surface roughness.

In process (3), not only the breaking probability but also the scale of wave breaking, which is shown typically as the scale of turbulent disturbance generated by wave breaking, will increase with wind speed and contribute to increase sea surface roughness. As regards the effect of the scale of wave breaking on the sea surface roughness more discussions will be given in Sect. 5.3.

In connection with the above discussions, Yelland and Taylor (1999) presented an interesting result that the relation between the drag coefficient C_D over sea surface and the 10 m height wind speed U_{10} depends on fetches (lake, coastal area, open ocean), and C_D is generally larger for shorter fetches. This is quite natural, because wave steepness for shorter dimensionless fetch is larger than that for longer dimensionless fetch as shown in Eq. (5), and wind waves in shorter dimensionless fetch tend to break earlier than those in longer dimensionless fetch.

5.2.4 Application to oceanographic phenomena

In applying the present results to the oceanographic phenomena we need to take care that the present results are obtained by using laboratory data where wind waves are fetch-limited and in an equilibrium state. In many cases, however, ocean waves are not always fetch-limited or in a local equilibrium state because of the spatial and temporal variability of the sea surface wind.

An example of breaking waves in the open ocean is shown in Fig. 8. The photo was taken in the North-Western Pacific Ocean during a wave observation by using a cloverleaf buoy (Mitsuyasu et al. 1975). We can see complex structure of breaking waves in the ocean probably because the wind and waves are not in a local equilibrium state as a result of temporal fluctuation of wind speed. Furthermore, in some cases, swell and ocean current will affect the wave breaking in the ocean.

Such complicated conditions in the ocean lead to a considerable scattering of the relation between the wind speed and the breaking probability or the sea surface roughness, while essential results are not much different from those obtained by controlled experiment.

Fig. 8 Breaking waves in the North-Western Pacific Ocean during wave observations using a clover-leaf buoy (Mitsuyasu et al. 1975). Wind speed U_{10} is about 9 m/s, mean wave height is 1.5 m, and mean wave period is 6.2 s

5.3 Relation between u_* and high frequency wave spectrum

5.3.1 Structures of high frequency wind waves: photographic information

The comparison of Fig. 5a, b with Fig. 3 shows that the dependence of the spectral densities of high frequency wave components on the wind friction velocity u_* is quite similar to that of the wind speed U_{10} at 10 m height on the wind friction velocity u_*. The results suggest an intimate relation between the high frequency wave spectrum and the sea surface roughness. To clarify the dynamical process in this phenomenon, photos of wind wave surface under the action of the wind will provide a lot of information because we can estimate empirically the property of the airflow above the water surface from the detailed configuration of the wind wave surface. For this purpose we use here the photos taken in our earlier study (Mitsuyasu and Honda 1975), because we did not take photos of wind wave surfaces in the present study. The earlier experiment was performed in a different (smaller) wind-wave tank, but measurements were done in a similar wind-speed range: $U_r = 5$, 7.5, 10, and 12.5 (m/s). Although the measurements of wind and waves were made at various fetches in the earlier study, here we use the data obtained at the fetch $X = 8.25$ m, which is comparable to the present fetch $X = 9.3$ m.

From their similarity properties, wind waves generated in different wind-wave tanks are almost the same if the wind speeds and fetches are the same and wind waves are deep water waves. The photos of wind waves and the corresponding frequency spectra in the earlier study are reproduced in Figs. 9 and 10. As expected, the earlier wind wave spectra shown in Fig. 10 are quite similar to the present ones shown in Fig. 4. Furthermore, the earlier data of u_* and U_{10}, which are shown in Table 1 in the earlier paper (Mitsuyasu and Honda 1975), fit to the present relation between u_* and U_{10}.

Looking closely at the photos shown in Fig. 9 we can see the following properties of wind waves growing under the action of the wind.

$U_r = 5$ m/s ($u_* = 0.26$ m/s): We can see steepening and forward inclination of the dominant waves. The wave form is quite similar to a spilling breaker under the action of strong surface tension which is shown in Fig. 1 of Duncan (2001). Bulge, toe, and capillary waves due to the instability mechanism (Longuet-Higgins 1963) are also seen. Waves are 3-dimensional and random. Wave breaking is not clear but some waves seem to be microscale breakers.

$U_r = 7.5$ m/s ($u_* = 0.51$ m/s): Clearly waves are spilling breakers. Turbulent disturbances generated by wave breaking can be seen at the crest of the dominant wave and they co-exist with capillary waves. Streamwise streaks (Ebuchi et al. 1987) are observed on the backward face of the waves.

$U_r = 10$ m/s ($u_* = 0.67$ m/s): Turbulent disturbances generated by wave breaking cover almost the entire wave surface and they co-exist with capillary waves.

$U_r = 12.5$ m/s ($u_* = 0.84$ m/s): We can clearly see the increases of wave steepness and turbulent disturbances of large scale at the wave crest.

$U_r = 15$ m/s ($u_* = 1.80$ m/s): Every phenomenon that appeared at the wind speed $U_r = 12.5$ m/s is greatly intensified and the entire water surface becomes very rough. Entrainment of the air bubble becomes remarkable.

From the photos of wind wave surface shown in Fig. 9 and typical properties of the wind wave surface described above, we can derive the following image on the dynamical process at the air–sea boundary. The separation of airflow at the wave crest will start at least at the wind speed $U_r = 7.5$ m/s ($u_* = 0.51$ m/s): the turbulent disturbance at the wave crest generated by small-scale wave breaking triggers airflow separation. Wind waves for $U_r = 5$ m/s ($u_* = 0.26$ m/s) are in a delicate situation: weak separation or no separation. It will be natural to consider that the critical wind speed is around this wind speed.

For the wind speed $U_r \geq 10$ m/s, the wind will separate on a large scale at the crest of dominant waves and the scale of separation will increase with wind speed as a result of the increase in the scale of the turbulent disturbance at the wave crest. This inference is supported indirectly by a laboratory study by Bandou and Mitsuyasu (1989). They studied the effect of artificial roughness at the crest of a solid wave on the airflow over the solid wave surface and found that the form drag due to the artificial roughness increases with the roughness size.

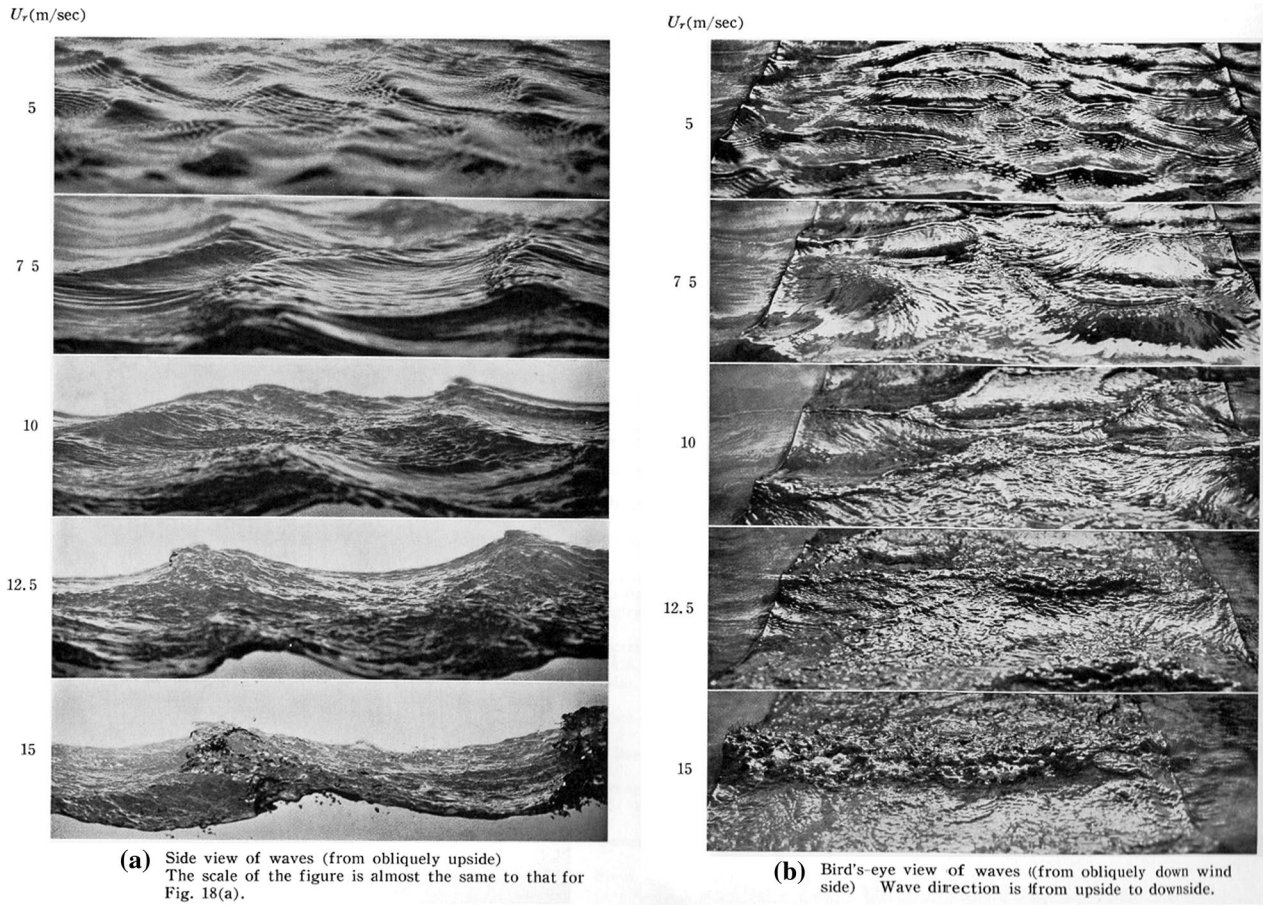

Fig. 9 Photographs of laboratory wind waves under the action of various wind speeds (from Mitsuyasu and Honda 1975). Reference wind speed and friction velocity U_r (u_*) m/s: 5 (0.26), 7.5 (0.51), 10 (0.67), 12.5 (0.84), 15 (1.80) from *top* to *bottom*. The fetch (at the *center* of the photos) is 8.25 m. The scales of the photos on the *left side* are changed respectively to see the details of the wind wave surface, and the widths of the photos correspond approximately to 0.27, 0.27, 0.38, 0.38, and 0.67 m from *top* to *bottom*. Directions of the wind and wave propagation are from *right* to *left*. The width of the photos on the *right side* corresponds roughly 0.6 m (width of the tank). Directions of the wind and waves propagation are from *upside* to *downside*

5.3.2 *Dynamical structure of the high frequency wave spectrum*

Complex patterns of wind wave surface covered with turbulent disturbances as shown in Fig. 9 bring about the following image of the structure of the high frequency wave spectrum shown in Fig. 10. Wave spectral density in a high frequency region, say $f > 3\,f_m$, corresponds largely to turbulent disturbances generated by wave breaking rather than high frequency free waves. Here f_m is a spectral peak frequency. If this image is realistic we can easily explain the relation between the sea surface roughness and the high frequency wave spectrum. Although there have been no studies thus far to confirm this image, the following study offers some support for this image. Kuo et al. (1979) studied the dispersion relation of laboratory wind waves. According to their study spectral components in the frequency range $f < 2\,f_m$ approximately satisfied a linear dispersion relation under the correction of the effect of surface drift current: high frequency waves in this region are really free water waves. However, frequency components in the region $f \geq 2\,f_m$ were dominated by nonlinear bound waves and high frequency free waves were difficult to detect. It will be an important future problem to clarify the dynamical structure corresponding to the high frequency part of the wind wave spectrum.

5.3.3 *Transitions in sea surface roughness and high frequency wave spectrum: future problems*

From the measured results and their discussions described above we can derive a possible but not confirmed explanation for the transitions of sea surface roughness and high frequency wave spectrum, which commonly appears at the wind speed $u_* = 0.2$ m/s. The explanation is as follows. With the start of small-scale wave breaking near the

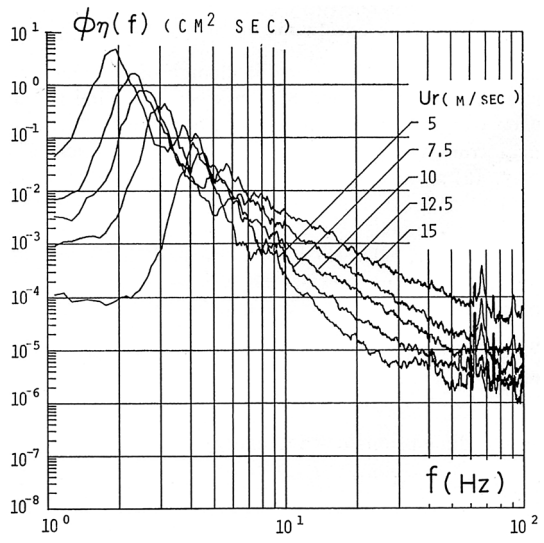

Fig. 10 Evolution of frequency spectrum of wind waves with wind speed at the fetch $X = 8.25$ m. The frequency spectra correspond to the waves in Fig. 9 (from Mitsuyasu and Honda 1975)

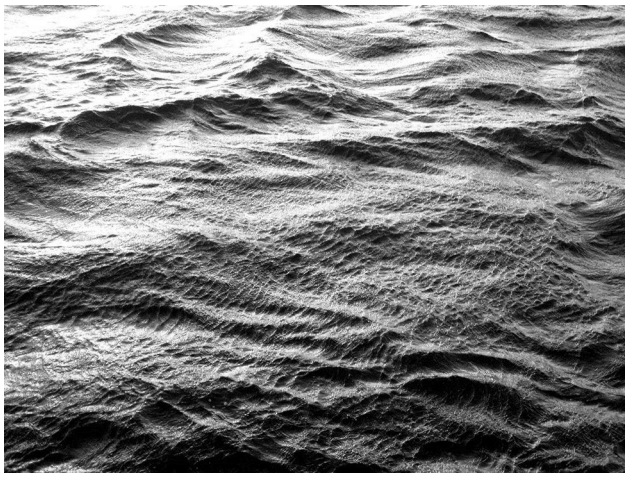

Fig. 11 Generation of capillary waves on the wind wave surface presumably due to the Kelvin–Helmholtz instability. Wind speed at 2 m height is roughly 8 m/s. The scale of dominant wind waves is roughly $H \sim 0.1$ m, $L \sim 1$ m. Directions of the wind and wave propagation are from right to left

critical wind speed, small turbulent disturbances are generated at the wave crest, and they trigger the separation of the airflow at the wave crest, and lead the sea surface roughness from smooth to rough. Such a dynamical process will correspond to the transition in the sea surface roughness. The scale of the turbulent disturbances increases with the increase of wind speed. The turbulent disturbances with large scale will contribute to changing the high frequency wave spectrum, too.

However, the above explanations are indirect and qualitative, largely because they are based mainly on the visual information from photos of wind waves. In order to clarify the phenomena quantitatively, accurate measurement and visualization of the airflow above wind waves are required, along with the measurement of the fine structure of growing wind waves. For example, we need to clarify the gradual change of breaking patterns of wind waves with the increase of wind speed by using optical technique (e.g., Ebuchi et al. 1987) or high-speed photographic techniques (e.g., Duncan et al. 1994), and associated change of wind structure over wind waves, such as the separation process and its statistics, say, by using traditional visualization techniques (e.g., Kawai 1983) or modern DPIV techniques (e.g., Reul et al. 2008).

5.4 Effects of capillary waves due to Kelvin–Helmholtz (K–H) instability

When Munk (1947) proposed the existence of a critical wind speed, he attributed the phenomenon to the change of sea surface roughness caused by capillary waves due to the K–H instability. This idea is very clear and interesting, but not confirmed as far as the author knows.

We can sometimes see the generation of capillary waves under the action of gusty high speed wind ($U_{10} \geq 7$ m/s), which may be attributable to the K–H instability. An example is shown in Fig. 11, where we can see capillary waves overlapping on a wide area of wind wave surface. The photograph was taken at a small fishing port when gusty wind of about 8 m/s at 2 m height is blowing. As a result of the short fetch, wind waves were small ($H \sim 0.1$ m, $L \sim 1$ m). At that time the capillary waves were very sensitive to the wind speed; if the wind speed increased the capillary waves were generated instantaneously but they attenuated quickly if the wind speed dropped down a little.

In open sea too we can see sometimes capillary waves overlapping on dominant waves when strong wind is blowing over the sea surface. A good example is seen in a photo shown on the front cover of the book *The Turbulent Ocean* by Thorpe (2005). Such capillary waves are different from those on front faces of dominant waves (Fig. 9), which are generated by an instability mechanism of steep waves (Longuet-Higgins 1963).

In spite of such evidence, when we regard their sporadic generation and relatively low wave heights, such capillary waves are difficult to regard as a dominant factor which triggers the airflow separation and contributes to the transition of sea surface roughness. Further studies are needed, however, on their generation, properties, and contributions to air–sea boundary processes, because our knowledge about such capillary waves, particularly their aerodynamic effect on sea surface wind, is meager. In many cases wind waves are generated by much lower wind speed

and develop before the generation of capillary waves by the K–H instability. That would have made the studies on the K–H instability in the water surface difficult.

6 Conclusions

We have discussed a critical wind speed for air–sea boundary processes by using our data on wind and wind waves, which have shown a kind of transition in the sea surface roughness and also in the high frequency components of the wind wave spectrum, which appear commonly near the wind speed $u_* = 0.2$ m/s ($U_{10} \fallingdotseq 8$ m/s). The conclusion is that the transition in the air–sea boundary processes near the critical wind speed exists and it will be attributed to the start of wave breaking. However, the critical wind speed is not a definite value; it scatters around the wind speed, say $u_* = 0.2$ m/s, due to the stochastic properties of breaking wind waves.

Dynamical processes for the phenomena can be considered as follows. For wind speed $u_* \leq 0.2$ m/s ($U_{10} \lesssim 8$ m/s), the water surface is almost smooth aerodynamically even though small wind waves are generated. Near the critical wind speed, $u_* = 0.2$ m/s ($U_{10} \fallingdotseq 8$ m/s), wind waves start to break and water surface roughness changes from smooth to rough. For the wind speed $u_* \geq 0.2$ m/s ($U_{10} \gtrsim 8$ m/s), the intensity of the wave breaking increases with wind speeds generating a growing disturbance at the wave crest: such a process leads to the gradual increase of water surface roughness and high frequency components of the wind wave spectrum. Melville (1977) presented a similar conclusion that the transition from smooth to rough flow is concomitant with the onset of small-scale wave breaking, and occurs in the neighborhood of $u_* = 0.23$ m/s.

The similarity between the wind-speed dependence of the sea surface roughness and that of high frequency components of the wind wave spectrum suggests the possibility that the high frequency components of the wind wave spectrum are largely contributions from breaking disturbances rather than high frequency components of wind waves. To confirm the suggestion is a future problem.

The effects of capillary waves due to the K–H instability are difficult to regard as a dominant factor which triggers the transition of the sea surface roughness. Further studies are needed, however, on their generation, properties, and contributions to the air sea boundary processes, because our knowledge on such capillary waves is meager.

Finally one thing needs to be noted. The present discussions and conclusions are largely based on the results of our laboratory experiments where the wind is stationary and wind waves are fetch-limited and in a local equilibrium state. In the ocean, however, wind waves are not always fetch-limited or in a local equilibrium state because of the temporal and spatial changes of wind speed on various scales. Such a realistic situation sometimes complicates the phenomena in the ocean.

Acknowledgments The author would like to express sincere thanks to Steve Thorpe, Professor Emeritus of Southampton University, for his critical reading of the manuscript and valuable suggestions. Professor Masuda provided insightful comments on the revised manuscript, Professor Mizuno helped to prepare the figures in the revised manuscript, and Dr. Sugihara provided valuable comments on an early draft of the paper. The author is grateful to two anonymous referees for their careful reading of the manuscript.

References

Babanin AV (2009) Breaking of ocean surface waves. Acta Phys Slovaca 59(4):305–535

Babanin AV, Young IR, Banner ML (2001) Breaking probability for dominant surface waves on water of finite constant depth. J Geophys Res 106(C6):11659–11675

Bandou T, Mitsuyasu H (1989) The structure of turbulent air flow over wavy wall, Part 3. Rept Res Inst Appl Mech Kyushu Univ 35(10):35–53

Banner ML (1990) The influence of wave breaking on the surface pressure distribution in wind-wave interaction. J Fluid Mech 211:463–495

Banner ML, Melville WK (1976) On the separation of air flow over water waves. J Fluid Mich 77:825–842

Banner ML, Babanin AV, Young IR (2000) Breaking probability for dominant waves on the sea surface. J Phys Oceanogr 30:3145–3160

Deacon EL, Webb EK (1962) Small scale interactions. In: Hill MN (ed) The sea, vol 1. Interscience, New York, pp 43–87

Duncan JH (2001) Spilling breakers. Annu Rev Fluid Mech 33:519–547

Duncan JH, Philomin V, Behres M, Kimmmel J (1994) The formation of spilling breaking water waves. Phys Fluid 6:2558–2560

Ebuchi N, Kawamura H, Toba Y (1987) Fine structure of laboratory wind-wave surfaces studied using an optical method. Bound-Layer Meteorol 39:133–151

Hara T, Bock EJ, Lyzenga D (1994) In situ measurements of capillary-gravity wave spectra using a scanning laser slope gauge and microwave radars. J Geophys Res 99(C6):12593–12602

Holthuijsen LH, Herbers THC (1986) Statistics of breaking waves observed as whitecaps in the open sea. J Phys Oceanogr 16:290–297

Jähne B, Riemer KS (1990) Two-dimensional wave number spectra of small-scale water surface waves. J Geophys Res 95(C7):11531–11546

Jones ISF, Toba Y (eds) (2001) Wind stress over the ocean. Cambridge University Press, Cambridge, p 307

Kawai S (1983) Structure of the air flow over wind wave crests revealed by flow visualization techniques. Bound-Layer Meteorol 23:503–521

Kinsman B (1965) Wind waves, their generation and propagation on the ocean surface. Prentice-Hall, Englewood Cliffs, p 676

Kunishi H, Imasato T (1966) On the growth of wind-generated waves in a high-speed wind flume. Disaster Prevention Research Institute, Kyoto University, Annual Report No. 9, pp 667–676

Kuo Y-Y, Mitsuyasu H, Masuda A (1979) Experimental study on the phase velocity of wind waves, Part 1 Laboratory wind waves. Rept Res Inst Appl Mech Kyushu Univ 27(83):1–19

Kusaba T, Masuda A (1988) The roughness height and drag law over the water surface based on the hypothesis of local equilibrium. J Oceanogr Soc Japan 44:200–214

Lamb H (1932) Hydrodynamics, 6th edn. Dover, New York, p 738

Longuet-Higgins MS (1963) The generation of capillary waves by steep gravity waves. J Fluid Mech 16:138–159

Melville WK (1977) Wind stress and roughness length over breaking waves. J Phys Oceanogr 7:702–710

Miles JW (1959) On the generation of surface waves by shear flows, Part 3: Kelvin–Helmholtz instability. J Fluid Mech 6:583–598

Miller BI (1964) A study of the filling of Hurricane Donna (1960) over land. Mon Weather Rev 92:389–406

Mitsuyasu H (1985) Recent studies on ocean wave spectra. In: Niordson FI, Olhoff N (eds) Theoretical and applied mechanics. Proc. 16th ICTUM. North-Holland, pp 249–261

Mitsuyasu H (1998) A note on the relation between wind speed and microwave sea return. In: Proc. PORSEC-'98 in Qingdao, pp 366–369

Mitsuyasu H, Honda T (1974) The high frequency spectrum of wind-generated waves. J Oceanogr Soc Jpn 30:185–198

Mitsuyasu H, Honda T (1975) The high frequency spectrum of wind-generated waves. Rep RIAM Kyushu Univ 22(71):327–355

Mitsuyasu H, Honda T (1986) The effect of surfactant on certain air-sea interaction phenomena. In: Phillips OM, Hasselmann K (eds) Wave dynamics and radio probing of ocean surface. Plenum, New York, pp 95–115

Mitsuyasu H, Kusaba T (1984) Drag coefficient over water surface under the action of strong wind. Nat Disaster Sci 6(2):43–50

Mitsuyasu H, Kusaba T, Marubayashi K, Ishibashi M (1992) The microwave backscattering from wind waves. Proc PORSEC-'92 in Okinawa, vol 1, pp 381–386

Mitsuyasu H, Tasai F, Suhara T, Mizuno S, Ohkusu M, Honda T, Rikiishi K (1975) Observation of the directional spectrum of ocean waves using a cloverleaf buoy. J Phys Oceanogr 5:750–760

Munk WH (1947) A critical wind speed for air–sea boundary processes. J Marine Res 6:203–218

Phillips OM (1977) The dynamics of upper ocean. Cambridge University Press, Cambridge, p 336

Reul N, Branger H, Giovananjeli J-P (2008) Air-flow structure over short-gravity breaking water wave. Boundary Layer Metrol 126:477–505

Smith SD (1988) Coefficient of sea surface wind stress, heat flux and wind profiles as a function of wind speed and temperature. J Geophys Res 93:15467–15474

Sugihara Y, Tsumori H, Ohga T, Yoshioka H, Serizawa S (2007) Variation of whitecap coverage with wave-field conditions. J Mar Syst 66:47–60

Thorpe SA (2005) The turbulent ocean. Cambridge University Press, Cambridge, p 439

Thorpe SA, Humphries PN (1980) Bubbles and breaking waves. Nature 283(31):463–465

Yelland MJ, Taylor PK (1996) Wind stress measurements from the open ocean. J Phys Oceanogr 26:541–558

Yelland MJ, Taylor PK (1999) Does the wind stress depend on the sea state? In: Sajjadi SG, Thomas NH, Hunt JCR (eds) Wind-over-wave coupling. Oxford University Press, Oxford, pp 107–117

Zao D, Toba Y (2001) Dependence of whitecap coverage on wind and wind-wave property. J Oceanogr 57:603–616